

LETTER

Open Access



Overcoming delamination in two-photon lithography for improving fabrication of 3D microstructures

Cheol Woo Ha^{1*}

Abstract

Two-photon lithography has emerged as a highly effective method for fabricating intricate three-dimensional (3D) microstructures. It enables the rapid fabrication of 3D microstructures, unlike conventional two-dimensional nanopatterning. Researchers have extensively investigated two-photon polymerization (TPP) for the fabrication of diverse 3D micro/nanodevices with high resolution. TPP can be applied in cell cultures, metamaterials, optical materials, electrical devices, and fluidic devices, to name a few. In this study, we investigate the applications and innovative research pertaining to TPP, which is an effective fabrication technique with significant advancement in various fields. In particular, we attempt to determine the reasons that cause the detachment or delamination of 3D microstructures during the development process and propose some solutions. A step-by-step fabrication process for a glass substrate, from photoresist deposition to laser scanning and the dissolution of the uncured photoresist, is presented. Defects such as pattern delamination are discussed, with emphasis on the cell scaffold structure and microlens array. Understanding and addressing these defects are vital to the success of 3D microstructure fabrication via TPP.

Keywords two-photon lithography, 3D microstructure, swelling, delamination, fabrication yield improvement

Introduction

Two-photon lithography (TPP) is a prominent and effective approach for the fabrication of intricate three-dimensional (3D) microstructures. Compared with conventional two-dimensional nanopatterning technology, TPP presents distinct advantages in terms of its ability to rapidly fabricate 3D microstructures. Researchers have extensively investigated the potential of TPP as a method for fabricating various complex 3D micro/nanodevices owing to its ability to achieve high resolutions.

TPP relies on the confined photoinitiation of polymerization facilitated by nonlinear optical processes. In this process, the photosensitizer absorbs two near

infrared photons and emits ultraviolet photons, thus initiating polymerization. This highly confined polymerization occurs within the focus of a tightly focused laser beam, which is achieved using a high numerical aperture lens in the fabrication system. The laser, with a wavelength range of 600–800 nm, exposes the photoresist, which cross-links at a light wavelength of approximately 400 nm. Polymerization is initiated when the focused laser beam exposes the photoresist, and the resulting solidified image of the focal spot is known as a voxel (volume pixel). By manipulating the laser focus via the designed laser path using a piezo stage or galvano scanner, the voxels are joined together, thus resulting in a final 3D structure. TPP has been widely applied across various domains, which demonstrates its versatility and efficacy. In particular, TPP has been applied in robotics [1–3], metamaterials [4–6], optical materials [7, 8], electrical devices [9, 10], and fluidic devices [11]. Furthermore, significant developments of diverse biodevices have been achieved through the application of TPP, as

*Correspondence:

Cheol Woo Ha
cwha@kitech.re.kr

¹ Advanced Joining and Additive Manufacturing R&D Department, Korea Institute of Industrial Technology, 113-58, Seohaean-Ro, Siheung 15014, Republic of Korea

evidenced by the successful commercialization of biomaterials (Fig. 1f) [12–14]. Moreover, TPP enables a vast array of optical devices to be achieved that offer exceptional adaptability and design freedom, thus rendering the use of masks (as in conventional lithography) unnecessary. This capability is visually exemplified in Fig. 1g, which shows a myriad of innovative optical devices. TPP is an effective and versatile fabrication technique in various fields.

As shown in Fig. 1a, the stereolithography process uses a femtosecond laser with an ultrashort pulse duration of 100 fs or less as the laser light source. Additionally, it uses an oil-immersion objective lens ($100\times$) with an aperture of 1.4 to focus and cure the laser onto a photocurable polymer resin. Using the laser focus, the cured areas can be individually connected to form a 3D shape. The photocurable polymer resin is manufactured by controlling the laser scanning in the x-, y-, and z-axis directions using an XYZ piezo stage with a resolution of 0.1 nm or less, adjusting the laser focus using a CCD camera with a high magnification lens, and monitoring the manufacturing process in real time. The area locally hardened at the laser focus is known as a voxel (volume of pixels). In stereolithography, voxels are superimposed via laser scanning to create a 3D shape. The shape of the voxel is determined by the laser power and laser scanning speed. Based on using these two parameters as the process variables, the process conditions can be determined by evaluating the pattern yielded by curing the polymer resin.

The step-by-step workflow of the fabrication process is shown in Fig. 1a, which provides a comprehensive understanding of the entire procedure conducted on a glass substrate. First, a drop of photoresist is deposited precisely onto the substrate, which is a preparatory step before TPP process. Subsequently, the prepared substrate and deposited photoresist are carefully inserted into a dedicated TPP machine. 3D microstructures are fabricated during the TPP process with the laser scanning. After the TPP process is completed, the uncured photoresist is dissolved, which is accomplished using an appropriate developing solution. Finally, the intended 3D microstructure is achieved.

Previously, researchers of TPP have focused on single-pattern fabrication. However, owing to the commercialization of the TPP technology, research into mass production via TPP has become increasingly important [15–18]. To achieve mass production, yield improvement is particularly important. To improve yield, defects that occur during patterning must be minimized. However, defects typically occur in TPP because of pattern delamination. The structure depicted in the Fig. 2a, b represents a cell scaffold. The fabrication time was approximately 30 min. However, this structure delaminated and detached from the glass substrate during development. It was designed to be fabricated as shown in Fig. 2b. However, only at a laser power of 50 mW, the microstructure was fabricated successfully. At

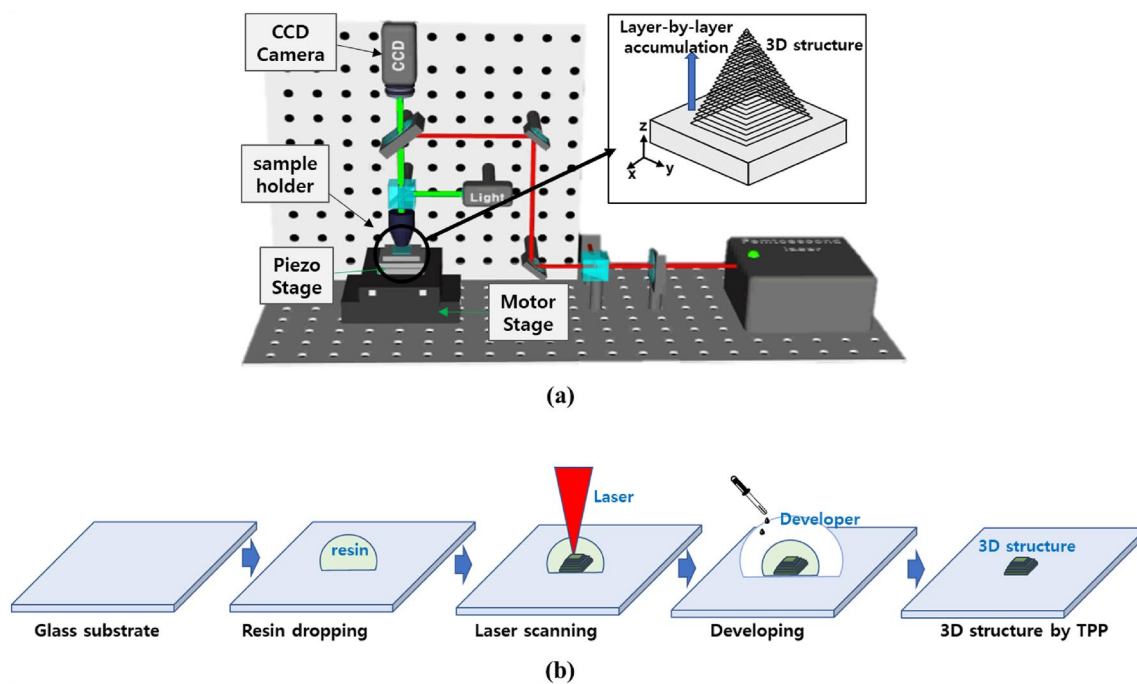


Fig. 1 **a** Configuration and conceptual diagram of two-photon lithography process equipment for fabrication of 3D microstructure. **b** Conceptual diagram showing overall process from resin deposition to development process for fabricating 3D microstructure via two-photon lithography

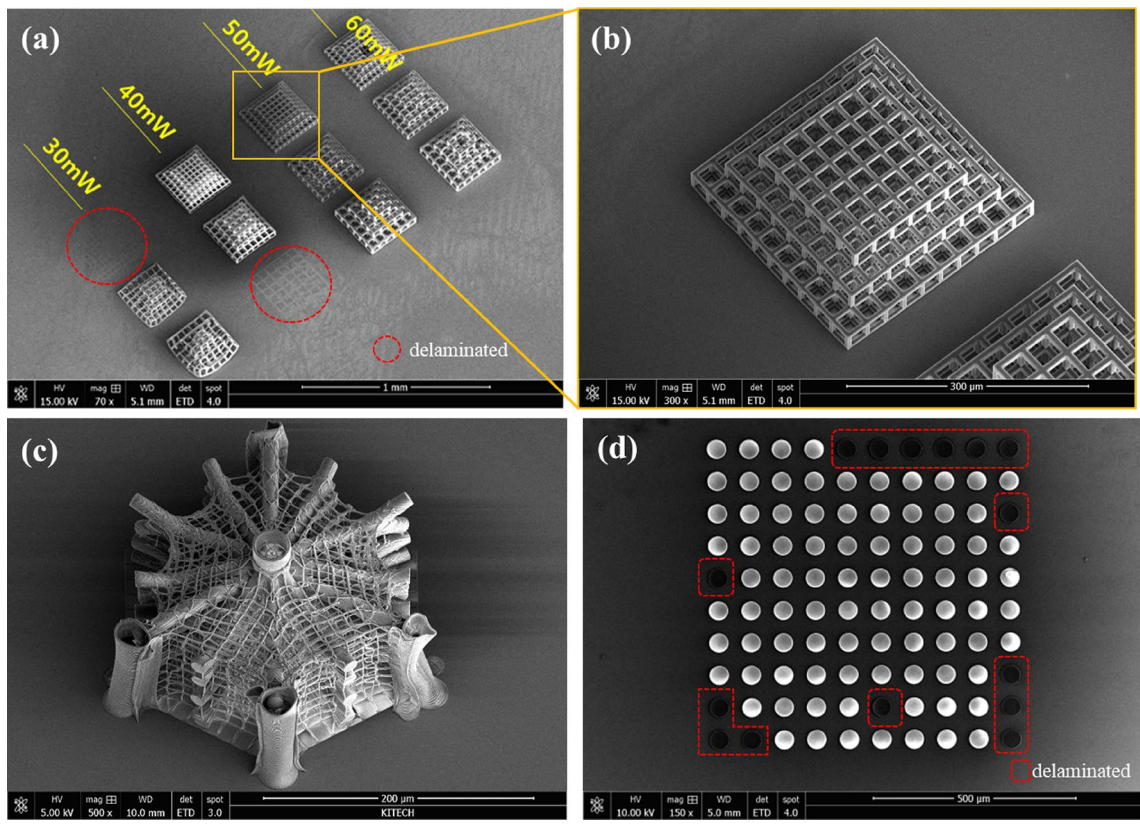


Fig. 2 SEM images showing various 3D microstructures fabricated via TPP. **a** 3D cell culture scaffolds for cell culture application. SEM image of 3D cell culture scaffold based on laser powers of 30, 40, 50, and 60 mW for the same structural design. At 30 and 40 mW, some of the structures were detached via delamination. **b** SEM image of one of cell culture structures. **c** Cell scaffold usable for cell culture applications. The pillars on the outer shell and the pillars that cross the inside of the scaffold are designed to mimic blood vessels. **d** SEM image of a microlens array, where some microlenses detached via delamination

laser power of 30mW and 40mW, some of the microstructures were delaminated and fell off entirely. In particular, at 40 mW, there are traces of delaminated structure. Figure 2c shows that the total production time was about 10 h. Delamination and detachment of the this large microstructure could result in substantial cost and production time losses. Additionally, in a complex structure such as a microlens array, all lenses must be attached firmly to the substrate. Although all the lenses were attached well during fabrication, some of them were detached from the substrate during the development process (Fig. 2d). If any of the lenses were removed, then the entire structure would be functionally defective, even if the remaining structures were well fabricated on the substrate. Therefore, this study is performed to determine the reasons that cause the 3D microstructures fabricated via TPP to detach from the substrate during the development process, as well as to propose solutions to solve this issue.

Experimental

Materials

All chemicals used in this study were purchased from Sigma-Aldrich, unless otherwise specified. For the fabrication, we used a two-photon photopolymerizable resist, IP-Dip (Nanoscribe GmbH). The IP-Dip resist was optimized by the manufacturer with a refractive index of 1.52. The structure was developed by rinsing away the uncured photoresist with propylene glycol monomethyl ether acetate (PGMEA). PGMEA was purchased from Sigma-Aldrich.

Morphological characterization

Scanning electron microscopy (SEM) was employed to verify the surface quality of the 3D microstructures. In particular, SEM images were captured using an FE-SEM instrument (NNS-450, FEI Hong Kong Company). To enhance the image contrast and quality, the samples were coated with a thin layer (15–30 nm) of Cr using a sputter

coater. All SEM images were acquired under vacuum using a secondary electron detector under an accelerating voltage ranging from 1.0 to 1.5 kV. A low imaging voltage (< 10 kV) was applied to prevent structural damage. Optical microscopy (OM) was employed to assess the delamination and deformation behaviors of the 3D microstructures. OM images and videos were captured using an Inverted Routine Microscope (Axio Vert.A1; ZEISS, Germany).

Results and discussion

In this study, we assumed that the 3D microstructures detached from the substrate because they absorbed the surrounding solvent, thus resulting in the deformation of the internal structure. After the lithography process via laser scanning was completed, the photocurable resin was washed off using a developer via a development process that required 5–10 min. Consequently, the polymer was continuously dipped in and absorbed the developer solution during the development process. During this time, the 3D microstructures can absorb the surrounding solvent, which causes their internal structure to deform. These deformations allow the 3D microstructure to be removed from the glass substrate.

Structural deformation due to solvent absorption is explained more comprehensively next. A space known as the free volume exists within the cured polymer structure. Photocurable polymers are cured using a laser, and a free volume is formed between the polymer chains during this process. This free volume serves as a space for the absorption of solvents within the 3D microstructure during development. The amount of absorbed solvent varies depending on the free volume. As the solvent molecules are absorbed into the free volume, the polymer network deforms, which can cause geometric delamination (Fig. 3). There are several research works for details discussion about the mechanism of solvent-induced

swelling. When the less cured network undergoes the developing process, it becomes more susceptible to significant swelling. Small solvent molecules penetrate the polymer network, increasing its volume. At this point, the swelling amount decreases as the cross-link density increases. The cross-linking density according to the laser power was discussed in previous work [19, 20].

The structural deformation depending on the amount of the free volume was discussed in the previous paper. If the microstructure is fabricated using the same laser power, the level of cross-linking remains consistent. As the structure becomes thicker, it possesses an increased amount of free volume. Therefore, the solvent absorption and the swelling are more prominent in this thick structure. In addition, in the previous paper, the delamination phenomenon according to the free volume was evaluated by finite element method (FEM) simulation. The polymer pattern adheres to the glass substrate. Stresses arise from the differing strain values between the polymer pattern and the glass substrate. As previously discussed, a larger amount of free volume results in a higher strain value. This elevated strain induces significant stress within the structure. This stress predominantly concentrates at the pattern's edges, leading to delamination from those edges [21, 22].

In addition, as the curing degree of the photocurable resin increases, the interpolymer bonds become stronger, and the space inside the cured polymer decreases. This implies less room inside the cured polymer and thus less strain. Conversely, when the curing degree of the photocurable resin was low, the interpolymer bonds were relatively weak, and the space (i.e., free volume) inside the cured polymer increases. These internal spaces can absorb a significant amount of solvent, thus causing the polymer to deform.

Herein, we discuss the method to solve the delamination problem in 3D microstructures fabricated using

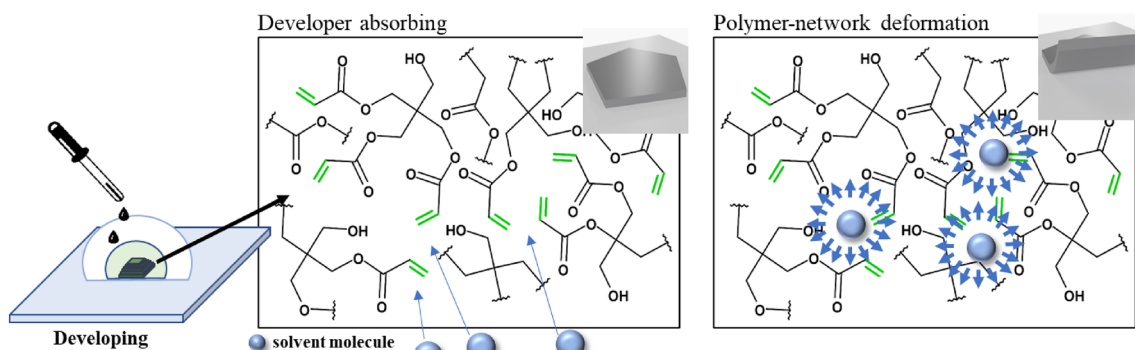


Fig. 3 Conceptual diagram showing absorption of solvent inside the polymer during development, which resulted in the expansion and deformation of the polymer-network inside the cured polymer

TPP. First, we consider whether the free volume within a 3D microstructure can be controlled through geometric design. The fabrication of 3D microstructures via TPP involves process and design variables. The process variables include the laser power and scanning speed. In TPP, voxels are overlapped through laser scanning to create a 3D microstructure [23–25]. As shown in Eq. 1, the size of the voxels is determined by the laser power and scanning speed, which are related to the laser energy required for photocuring. To simplify the experiment, the laser speed was fixed at 10 mm/s, and only the laser power was controlled [26, 27].

$$d(P, t) = \frac{\lambda}{\pi(\sin^{-1} NA/n)} \left[\ln \frac{4\pi^2 P^2 t \tan^4(\sin^{-1} NA/n)}{E_{th}\lambda} \right]^{\frac{1}{2}} \quad (1)$$

The design variables include the length and height of the 3D microstructure. Structures with various geometries can be designed by varying the stacking areas and heights. Herein, we simplify the 3D microstructure to a square plate to discuss the delamination caused by the free volume as a function of the design variables. Figure 4a shows the experimental results for verifying the effect of delamination on the microstructural area. In the experiment, the thickness of the square plate was fixed at 3 μm and the length was varied as 4, 8, 12, 16, 20, and 24 μm. SEM images of the fabricated structures showed that delamination occurred in all the structures, thus

indicating that the area of the fabricated structures was irrelevant for solving the delamination issue. As previously discussed, the amount of free volume determines the amount of solvent absorbed, and solvent absorption can cause the structure to deform. Because no improvement in delamination was observed with respect to area, the amount of free volume per unit volume is assumed to be related to delamination. In other words, when fabricating 3D microstructures using TPP, the free volume per unit volume is expected to decrease by increasing the curing degree of the photocurable polymer. Consequently, the delamination is expected to decrease.

Furthermore, the experimental results showed that delamination initiated primarily at the vertex, and once the delamination affected the microstructure at the vertex, it continued toward the other edges. The internal stresses caused by the absorption of the surrounding solvent into the polymer structure resulted in stress differences between the polymer and glass substrate. This stress difference was concentrated near the vertices of the square-plate structure; therefore, the square-plate structure began to delaminate from the vertices [21].

In addition, the delamination resolved when the laser power increased to a certain level. This is related to the change in free volume within a unit volume, i.e., as the laser power increases, the cross-linking between polymers in the photocurable resin becomes more activated, and the curing degree increases. This results in a smaller free volume, which is assumed to decrease the

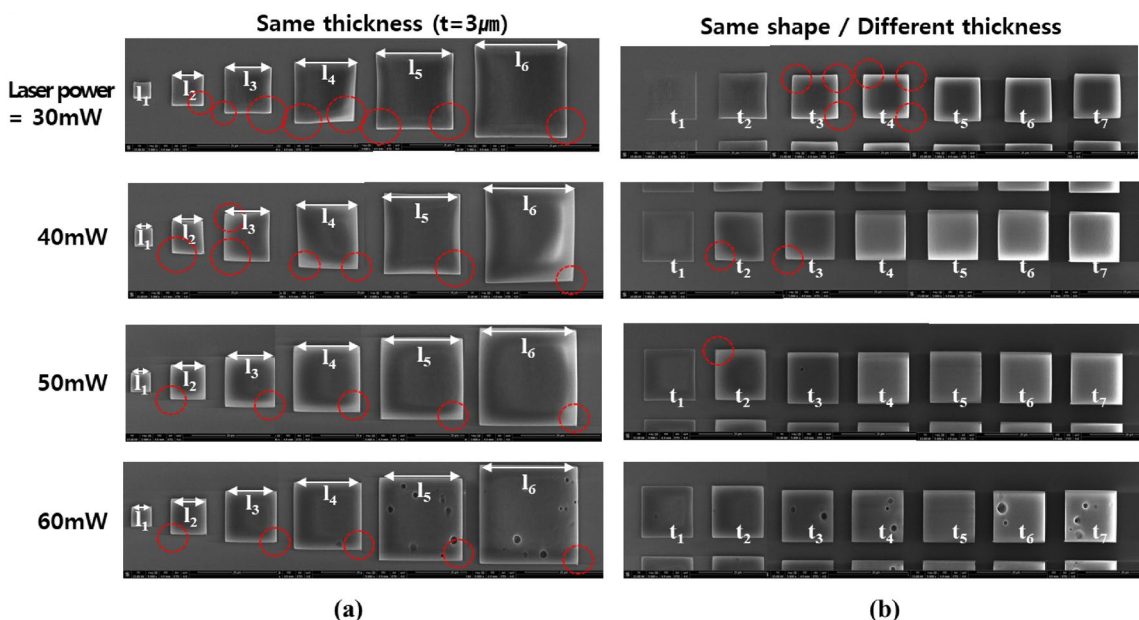


Fig. 4 SEM images showing correlation between delamination occurrence for different designs and different process conditions. **a** Delamination for different stacking areas (l) at the same thickness. ($l_1=4$, $l_2=8$, $l_3=12$, $l_4=16$, $l_5=20$, and $l_6=24$ μm) **b** Delamination for different thicknesses (t) at the same length ($l=12$ μm). ($t_1=1$, $t_2=2$, $t_3=3$, $t_4=4$, $t_5=5$, $t_6=6$, and $t_7=7$ μm). Red circles indicate the region of delamination

amount of solvent absorption and thus solve the delamination problem. This can be explained from two points of view. In Fig. 4, red circles have been placed where delamination is suspected to occur. It can be seen that as the laser power increases, the suspected delamination area is decreased. Also, by comparing the shapes of the patterns, it can be seen that delamination tends to decrease with increasing laser power. The pattern is designed with a square structure, but when delamination or deformation occurs due to swelling, the pattern becomes distorted. The pattern distortion can be easily seen at low power. However, as the laser power increases, the pattern becomes less distorted and remains in its original square shape.

However, in our experiments, we observed that when the laser power exceeded 60 mW, damage and bubbles occurred in the photocurable resin due to excessive laser power. Therefore, under a laser power of 60 mW, the fabrication of precise 3D microstructures is challenging because of bubbles generated in the resin. This suggests that the appropriate curing conditions should be established via the laser power. An extremely low power will not ensure the sufficient curing and accuracy of the structure, whereas an extremely high power will cause problems such as resin damage and bubbling.

As shown in Fig. 4b, we conducted an experiment to determine the effect of the thickness of the 3D microstructure on delamination. In the experiment, the length of the square plate was fixed at 12 μm to maintain a constant area, and the thickness of the fabricated shape was varied as 1, 2, 3, 4, 5, 6, and 7 μm . The experimental result shows that delamination occurred at small thicknesses but was alleviated as the thickness increased. The delamination was almost invisible at thicknesses exceeding 5 μm . Furthermore, delamination decreased gradually as the laser power increased, and almost no delamination was observed at 50 mW.

Based on these results, we discuss the delamination of the structures based on different areas, heights, and laser powers. At a laser power of 30 mW, shrinkage and delamination occurred under most of the lengths and thicknesses investigated. At a laser power of 40 mW, delamination occurred over most of the area; however, the delamination degree decreased as the thickness increased. At a laser power of 50 mW, delamination reduced significantly; however, at a laser power of 60 mW, polymer damage and bubbling were observed owing to the excessive laser energy. The overall results of these experiments suggest that delamination can be solved by setting the appropriate laser power and thickness. Specifying a sufficient thickness can significantly reduce delamination on the structure; however, using an extremely high laser power can cause polymer damage and bubble generation.

We discovered that the stacking area of the structure was not effective in reducing delamination, i.e., increasing the stacking area did not reduce delamination. However, we discovered that delamination was reduced as the thickness of the structure increased. This can be attributed to the increased bending stiffness of the structure. As illustrated in Fig. 5a, when the microstructure absorbs the surrounding solvent, the internal structure expands. Because the lower surface of the microstructure was fixed to the glass substrate, the microstructure deformed toward the top of the substrate. This deformation can be assumed to be the deformation (δ) of the cantilever caused by the external stress distribution (W), as shown in Fig. 5b. In this case, the deformation of a cantilever of length (L) can be expressed as shown in Eq. 2, which indicates that the deformation of the cantilever is determined by the bending stiffness (I). The bending stiffness can be expressed as shown in Eq. (3). Therefore, as the thickness (t) of the structure increases, the bending stiffness of the cantilever increases, and the amount of deformation in

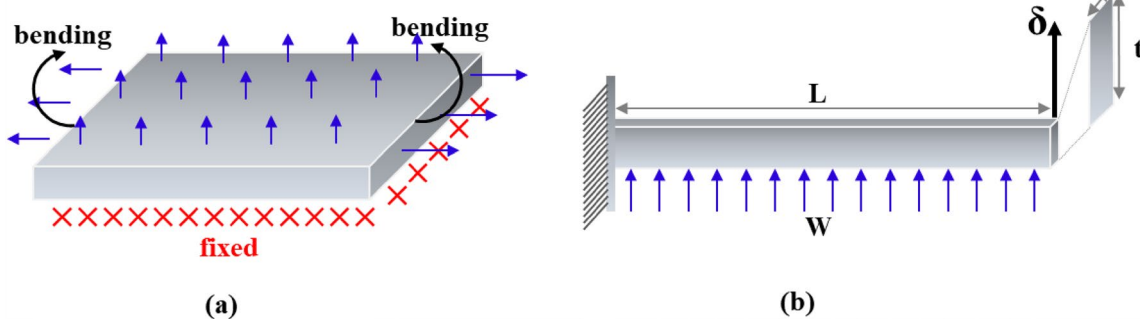


Fig. 5 **a** Conceptual diagram showing force distribution during deformation of square plate due to solvent absorption. **b** Conceptual diagram showing deformation of cantilever due to external stress distribution

the cantilever decreases accordingly. This implies that as the thickness of the structure increases, the deformation of the structure due to the internal expansion of the polymer decreases.

We discovered that the stacking area of the structure was not effective in reducing delamination, i.e., increasing the stacking area did not reduce delamination. However, we discovered that delamination was reduced as the thickness of the structure increased. The delamination reduction with increasing thickness will be discussed through mechanical structural analysis. This can be attributed to the increased bending stiffness of the structure. As illustrated in Fig. 5a, when the microstructure absorbs the surrounding solvent, the internal structure expands. The different strain values of the polymer pattern and the glass substrate generate stress. This stress is concentrated at the edges of the pattern, so delamination occurs at the edges of the structure [21]. Because the lower surface of the microstructure was fixed to the glass substrate, the microstructure deformed like concave structure. This phenomenon can be shown from the Fig. 4a. It can be assumed that the microstructure bended toward the top of the substrate.

Therefore, it can be approached as a bending problem of a mechanical structure under external stress. This bending deformation can be assumed to be the deformation (δ) of the cantilever caused by the external stress distribution (W). In Fig. 5a, the concave deformation force is assumed to be W as delamination occurs. It can also be assumed that the amount of deformation that occurs away from the substrate is δ (Fig. 5a). In general, the bending of a mechanical structure is expressed as Eq. 2. E is the Yong's modulus, which is a material property. L is related to the length of the structure, which is independent of the thickness of the structure. In this case, the deformation (δ) of the mechanical structure is determined by the bending stiffness (I). The center of the pattern is well adhered to the substrate without delamination. Therefore, if the center of the pattern is assumed to be fixed, the bending stiffness can be expressed as shown in Eq. (3). The thickness of the structure being discussed here is t , and the bending stiffness is proportional to t . Therefore, as the thickness (t) of the structure increases, the bending stiffness of the cantilever increases, and the amount of deformation in the cantilever decreases accordingly. This implies that as the thickness of the structure increases, the deformation of the structure due to the internal expansion of the polymer is decreased.

In addition, we experimentally observed that the delamination problem resolved as the laser power increased. As the laser power increased, the

photocuring reaction of the photocurable resin became more active, and the curing degree increased. Furthermore, as the laser power increased, the free volume decreased; therefore, shape deformation caused by the surrounding solvent decreased as the laser power increased. However, at a certain laser power (e.g., 60 mW), bubbles were generated in the polymer. These bubbles were caused by the evaporation of the solvent from the polymer by the high laser power. Therefore, in such cases, delamination can be solved by reducing the laser power and designing the appropriate heights for the 3D shape. Thus, we experimentally confirmed that delamination is governed by the thickness of the structure and the laser power, as indicated by the change in the bending stiffness and curing degree.

$$\delta = \frac{WL^2}{2EI} \quad (2)$$

$$I = \frac{xt^3}{12} \quad (3)$$

Additionally, the delamination problem was assessed on a pentagonal structure to determine the effect of the structural design. OM was performed to confirm the occurrence of delamination. Although SEM is useful for accurately imaging the geometry, OM more suitable for identifying delamination. When a 3D microstructure separates from the substrate owing to delamination, a microscopic space is created between the substrate and 3D microstructure. This microscopic space distorts the light path, as viewed under an optical microscope. Therefore, the delamination pattern can be accurately observed using an optical microscope. As shown in Fig. 6a, b, the same conclusions as those obtained for the square plate were obtained from the experiments involving the pentagonal structure, i.e., delamination decreased as the thickness of the structure increased, regardless of the length or area of the microstructure, and delamination was alleviated as the laser power increased.

Based on these experimental results, we successfully fabricated structures with improved delamination. Figures 6c–d shows the results of structures fabricated without delamination when the thickness of the pentagonal structure was 5 μm and the laser power was 45 mW. All the structures did not exhibit delamination. As the TPP process technology matures, mass production based on TPP will become increasingly important. Hence, the delamination defect improvement discussed herein is expected to facilitate yield improvement activities related to TPP.

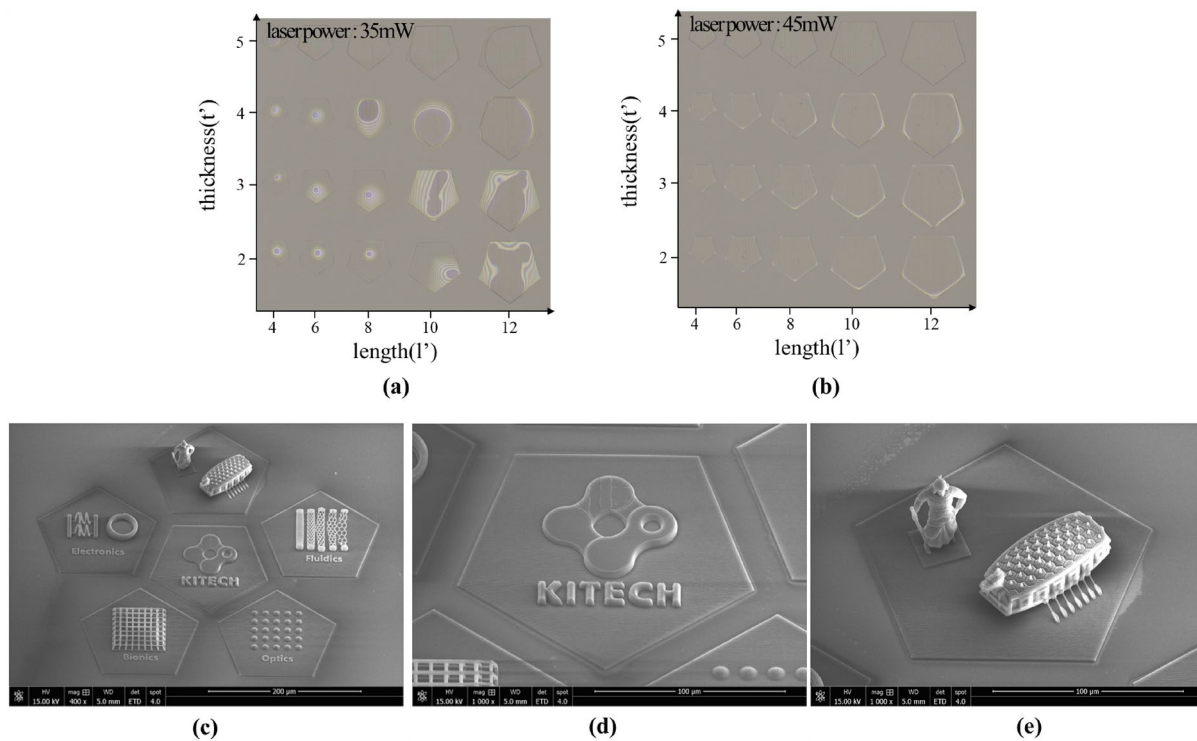


Fig. 6 Optical images showing delamination on pentagonal structures. Fabrication was performed under **a** 35 mW and **b** 45 mW of laser power. **c** SEM images of 3D microstructures fabricated based on the obtained pentagonal dimensions. Magnified SEM images of **d** KITECH symbol and **e** sculpture of Korean admiral Yi Sun-sin and the Turtle Ship

Conclusion

The delamination problem in 3D microstructures fabricated via TPP was discussed herein. The effects of the process variables (laser power and scanning speed) and design variables (length and height of the structure) on delamination were investigated. Basically, we discussed that delamination is caused by the absorption of the surrounding solvent into the internal free volume of the fabricated polymer, causing the structure to be distorted. One of the ways to mitigate delamination of 3D microstructures is to increase the laser power. By increasing the laser power, there is a lot of curing between the polymers. Consequently, a polymer network becomes denser. As a result, there is less free volume for the surrounding solvent to be absorbed and delamination is alleviated. However, an excessively high laser power resulted in polymer damage and bubbling. Increasing the thickness of the structure resulted in a higher bending stiffness and less deformation owing to solvent absorption, which alleviated delamination.

The results for both square and pentagonal structures were consistent, thus indicating that the geometries did not affect the outcomes. Using the appropriate laser power and thickness can effectively

reduce delamination. The results of this study provide valuable insights into the delamination problem encountered in 3D microstructures fabricated via TPP. As the TPP technology advances, the findings of this study are expected to facilitate yield improvement activities related to mass production via TPP.

Abbreviations

TPP	Two-photon polymerization
3D	Three-dimensional

Acknowledgements

Planck inc (www.planck.co.kr) is grateful for setting up the two-photon lithography process equipment and support for the two-photon lithography experiment.

Author contributions

CWH designed and conducted the overall experiment. He also analyzed the data and wrote all the manuscript. He also supervised the fundings of this work and reviewed the manuscript.

Funding

This work was supported by the Research Program (NRF-2020K1A3A1A19087858) of the National Research Foundation (NRF) of Korea. This work was also supported by the Korea Institute of Industrial Technology as an internal project (JH230014).

Availability of data and materials

All data generated or analyzed during this study are included in this published article.

Declarations

Consent for publication

Authors consent the SpringerOpen license agreement to publish the article.

Competing interests

The authors declare that they have no competing interests.

Received: 9 July 2023 Accepted: 3 September 2023

Published online: 22 September 2023

References

- Kim S, Qiu F, Kim S, Ghanbari A, Moon C, Zhang L, Nelson BJ, Choi H (2013) Fabrication and characterization of magnetic microrobots for three-dimensional cell culture and targeted transportation. *Adv Mater* 25(41):5863–5868
- Huang TY, Sakar MS, Mao A, Petruska AJ, Qiu F, Chen XB, Kennedy S, Mooney D, Nelson BJ (2015) 3D printed microtransporters: Compound micromachines for spatiotemporally controlled delivery of therapeutic agents. *Adv Mater* 27(42):6644–6650
- Ha CW, Yang D-Y (2014) Rotational elastic micro joint based on helix-augmented cross-spring design for large angular movement. *Optics Express* 22(17):20789–20797
- Tayalia P, Mendonca CR, Baldacchini T, Mooney DJ, Mazur E (2008) 3D cell-migration studies using two-photon engineered polymer scaffolds. *Adv Mater* 20(23):4494–4498
- Zheludev NI, Kivshar YS (2012) From metamaterials to metadevices. *Nature Mater* 11(11):917–924
- Espinosa-Hoyos D, Jagielska A, Homan KA, Du H, Busbee T, Anderson DG, Fang NX, Lewis JA, Van Vliet KJ (2018) Engineered 3D-printed artificial axons. *Sci Reports* 8(1):1–13
- Gissibl T, Thiele S, Herkommer A, Giessen H (2016) Two-photon direct laser writing of ultracompat multi-lens objectives. *Nature Photonics* 10(8):554–560
- Liu Y, Wang H, Ho J, Ng RC, Ng RJ, Hall-Chen VH, Koay EH, Dong Z, Liu H, Qiu C-W (2019) Structural color three-dimensional printing by shrinking photonic crystals. *Nature Commun* 10(1):4340
- Liu L, Yang D, Wan W, Yang H, Gong Q, Li Y (2019) Fast fabrication of silver helical metamaterial with single-exposure femtosecond laser photoreduction. *Nanophotonics* 8(6):1087–1093
- Ha CW, Prabhakaran P, Son Y (2019) 3D-printed polymer/metal hybrid microstructures with ultraprecision for 3D microcoils. *3D Print Additive Manufact* 6(3):165–10
- Vanderpoorten O, Peter Q, Challa PK, Keyser UF, Baumberg J, Kaminski CF, Knowles TP (2019) Scalable integration of nano-, and microfluidics with hybrid two-photon lithography. *Microsyst Nanoeng* 5(1):40
- Lee K-J, An JH, Shin J-S, Ha CW, Son Y, Seok J, Lee K-S (2017) Evaluation of anticancer drug in a polymer 3D cell chip. *Optical Mater Express* 7(8):2752–2759
- Claeyssens F, Hasan EA, Gaidukeviciute A, Achilleos DS, Ranella A, Reinhardt C, Ovsianikov A, Shizhou X, Fotakis C, Vamvakaki M (2009) Three-dimensional biodegradable structures fabricated by two-photon polymerization. *Langmuir* 25(5):3219–3223
- Huang F, Zhang J, Li T, Duan R, Xia F, Willner I (2018) Two-photon lithographic patterning of DNA-coated single-microparticle surfaces. *Nano Lett* 19(1):618–625
- Kim D, So PT (2010) High-throughput three-dimensional lithographic microfabrication. *Optics lett* 35(10):1602–1604
- Ritschdorff ET, Nielson R, Shear JB (2012) Multi-focal multiphoton lithography. *Lab Chip* 12(5):867–871
- Moon JH, Ford J, Yang S (2006) Fabricating three-dimensional polymeric photonic structures by multi-beam interference lithography. *Polymers Adv Technol* 17(2):83–93
- Maibohm C, Silvestre OF, Borme J, Sinou M, Heggarty K, Nieder JB (2020) Multi-beam two-photon polymerization for fast large area 3D periodic structure fabrication for bioapplications. *Sci Reports* 10(1):8740
- Zhang Q, Weng S, Hamel CM, Montgomery SM, Wu J, Kuang X, Zhou K, Qi HJ (2021) Design for the reduction of volume shrinkage-induced distortion in digital light processing 3D printing. *Extreme Mech Lett* 48:101403
- Zhao Z, Wu J, Mu X, Chen H, Qi HJ, Fang D (2016) Desolvation induced origami of photocurable polymers by digital light processing. *Macromol Rapid Commun* 38(13):1600625
- Woo HC, Maxime D, Jongsu K, Won CJ, Ji-Sun L, Jisu H, Si-Mo Y, Yong S, Xiangming C, Edavalath HN, Prem P (2021) 2D to 25 D transitions through controlled swelling delamination of hydrogel microstructures. *Mater Design* 212:110226
- Liu DX, Sun YL, Dong WF, Yang RZ, Chen QD, Sun HB (2014) Dynamic laser prototyping for biomimetic nanofabrication. *Laser Photonics Rev* 8(6):882–888
- Balena A, Bianco M, Pisanello F, De Vittorio M (2023) Recent advances on high-speed and holographic two-photon direct laser writing. *Adv Funct Mater*. <https://doi.org/10.1002/adfm.202211773>
- Ha CW, Prabhakaran P, Lee K-S (2019) Versatile applications of three-dimensional objects fabricated by two-photon-initiated polymerization. *MRS Commun* 9(1):53–66
- Prabhakaran P, Son Y, Ha CW, Park JJ, Jeon S, Lee KS (2018) Optical materials forming tightly polymerized voxels during laser direct writing. *Adv Eng Mater* 20(10):1800320
- Lee K-S, Kim RH, Yang D-Y, Park SH (2008) Advances in 3D nano/microfabrication using two-photon initiated polymerization. *Progress Polymer Sci* 33(6):631–681
- Ha CW, Prabhakaran P, Son Y, Lee K-S, Yang D-Y (2017) Effective direct writing of hierarchical 3D polymer micromeshes by continuous out-of-plane longitudinal scanning. *Macromol Res* 25:1129–1134

Publisher's Note

Springer Nature remains neutral with regard to jurisdictional claims in published maps and institutional affiliations.

Submit your manuscript to a SpringerOpen® journal and benefit from:

- Convenient online submission
- Rigorous peer review
- Open access: articles freely available online
- High visibility within the field
- Retaining the copyright to your article

Submit your next manuscript at ► springeropen.com